6-15-2007

Collapse analysis of nanofibers

Xiang-Fa Wu
Department of Engineering Mechanics, University of Nebraska-Lincoln, xfwu@unlserve.unl.edu

Yuris A. Dzenis
Department of Engineering Mechanics, University of Nebraska-Lincoln, ydzenis@unl.edu

Published in *Nanotechnology* **18** (2007) 285702 (6 pp); doi 10.1088/0957-4484/18/28/285702

Submitted January 18, 2007; revised April 22, 2007; published June 15, 2007.

Collapse analysis of nanofibers

Xiang-Fa Wu and Yuris A. Dzenis

Department of Engineering Mechanics, Nebraska Center for Materials and Nanoscience, University of Nebraska–Lincoln, Lincoln, NE 68588-0526, USA

Corresponding author — X.-F. Wu, email: xfwu@unlserve.unl.edu

Abstract

Continuous nanofibers fabricated by the electrospinning technique have found increasing applications (*e.g.*, nanofiber composites, nanofiber devices, bioengineering tissue scaffolding, etc.). For a nanofiber network subjected to a small external perturbation, the fiber segments within the network may deflect and stick to each other under the condition that their surface adhesion energy overcomes the elastic strain energy induced by fiber bending. Therefore, this paper aims to study adhesion-induced nanofiber collapse and relevant criteria. A simple fiber collapse model was proposed, which is based on the contact of two deflected elastic filaments under surface adhesion. Four fundamental fiber collapse modes (*i.e.*, fiber-flat substrate, parallel fibers, orthogonal fibers and fibers at arbitrary angle) were considered, and corresponding collapse criteria were determined in explicit forms. Effects of fiber elasticity, surface adhesion and fiber geometries on the collapse criterion were explored in a numerical manner. Results show that for a fiber segment pair at a relatively large angle, the critical distance to induce the fiber collapse is independent of the fiber radius. This distance is a function of the fiber aspect ratio and the material intrinsic length (γ/E, where γ is the surface energy and E is Young's modulus). The fiber collapse model developed in this study can be used as the theoretical basis for design and failure analysis of nanofiber networks and nanofiber devices, among others.

1. Introduction

Due to their porous properties with high surface area to volume ratio and tensile strength, fibrous materials have found extensive applications in thermal and sound insulators, gas and fluid filters, electromagnetic shields, chemical carriers, tissue templates, paper products, fibrous reinforcement in composites, etc. The effective properties of a fibrous material are a result of the properties of individual fibers, fiber arrangement, and bonding strength between neighboring fiber segments in contact. By comparison with their bulk counterparts, fibers typically have higher tensile strength that can be further enhanced with decreasing their diameters under proper spinning conditions. As a result, fiber networks made of ultrathin fibers (*e.g.*, nanofibers) are expected to bear preferable chemophysical and mechanical properties superior to those made of thicker fibers. Recently, ultrathin continuous fibers with diameters ranging from hundreds of nanometers up to a few microns have been fabricated successfully by means of the electrospinning technique [1–3]. As one of the novel nanomanufacturing methods, electrospinning is capable of producing clean and uniform ultrathin fibers from various precursors (*e.g.*, polymers, biomaterials, ceramics, etc). Figure 1 shows typical electrospun polyacrylonitrile (PAN) nanofibers with diameters around 300 nm. Furthermore, ultrathin fibers with diameters lower than 5 nm have also been produced successfully by electrospinning [4]. So far, continuous nanofibers have found rapidly growing applications in nanofiber composites [5–8], ultrafine filtration, chemical carriers [9], biomedical engineering and biological technology [9–11], among others.

In view of mechanics, fiber networks (assemblies) belong to heterogeneous material. Subjected to external loading, the global mechanical response of a fiber network depends upon the specific fiber arrangement, interaction between neighboring fibers (*e.g.*, contact, adhesion, friction, etc.) and the mechanical properties of individual fibers. For effective stiffness of fiber networks, remarkable progress has been made since the pioneering work by van Wyk [12] and Cox

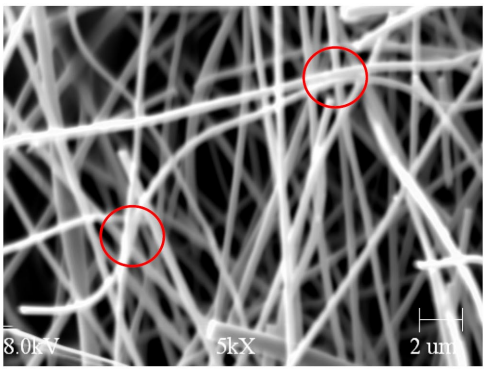

Figure 1. Adhesion between nanofibers within PAN nanofiber network (nanofiber diameter ~300 nm, circles indicate the adhesion zones).

[13]. Quite a few models [14–33] have been developed in the last two decades based on various assumptions of fiber deformations and fiber–fiber contacts. These models were largely validated in experiments and/or purely numerical simulations (*e.g.*, FEA). On the other hand, with decreasing fiber diameters, fiber rigidity decays rapidly and the fiber surface effect may play an appreciable role in the mechanical response of fiber networks such as effective stiffness, flexural rigidity, dynamic properties (*e.g.*, wave dispersion [34]), among others.

Consider a fiber network made of thin fibers subjected to small perturbation (*e.g.*, air flow). Neighboring fibers in the network may deflect and stick to each other due to their low flexural rigidity and appreciable surface adhesion. As a result, fiber collapse and adhesion vary the connectivity and topology of the fiber network, and may further lead to nonlinear behavior and even global collapse (*e.g.*, large area adhesion) of the fiber network. As a matter of fact, fiber collapse and adhesion definitely degrade the superior properties of fiber networks that are based on their unique fibrous geometries. Furthermore, nanofiber collapse and adhesion may even lead to the catastrophic failure of single nanofiber devices to be developed. Therefore, it is desired to explore the collapse mechanisms and relevant criteria in order to predict and therefore avoid the catastrophic failure of nanofiber networks and nanofiber devices. Nevertheless, to the authors' knowledge, no study has been reported yet in the literature to take into account nanofiber collapse.

Thus, in this work we initiate the study to consider surface adhesion-induced collapse and relevant criteria of thin fibers in a fiber network. A simple fiber collapse model is proposed, which is based on the contact of two deflected elastic cylindrical filaments involving surface energy. For the study of adhesion between elastic bodies, several pioneering models (*e.g.*, DMT, JKR, Maugis–Dugdale, etc.) have been proposed and validated in experiments [35–39]. Comparison among these models and their applications in MEMS/NEMS were reviewed in the recent literature [40, 41]. For our purpose, Bradley's approach [35] is to be employed for determining the adhesive force between neighboring fiber segments sticking at one point. Four fundamental collapse modes (*i.e.*, fiber-flat substrate, parallel fibers, orthogonal fibers and fibers at arbitrary angle) are to be considered. For each case, corresponding collapse criterion is obtained in explicit form. Effects of fiber elasticity, surface energy, and fiber geometries on the collapse criterion are explored in detail using a numerical manner. Potential applications of the present model in design and failure analysis of fiber networks and nanofiber devices are further addressed.

2. Problem statement and solutions

In this work, we are going to focus on the fiber collapse in a fiber network induced by surface adhesion between neighboring fiber segments. The typical nanofiber network formed in electrospinning is shown in Figure 1, in which PAN nanofibers stick together at some locations due to surface adhesion. Without loss of generality, two assumptions will be implied in the upcoming derivation to simplify the modeling process. First, each fiber segment is assumed to be fixed between neighboring contacts, and the contacts have no displacements during the deflection of fiber segments, *i.e.*, each fiber segment is considered simply as a fixed beam. Second, surface adhesion between neighboring fiber segments is assumed ideal, *i.e.*, fibers are dealt with as ideal elastic cylinders and effects of surface roughness and environmental factors (*e.g.*, moisture) are ignored. Therefore, in the present case of typical electrospun nanofibers with diameters over hundreds of nanometers, classic adhesion theories can be safely used. In this study, four fundamental fiber collapse modes are to be considered (*i.e.*, fiber-flat substrate, parallel fibers, orthogonal fibers and fibers at arbitrary angle), respectively, in which surface adhesion between fiber and flat substrate can be considered as the limiting case of the other three.

2.1. Collapse of nanofiber segment on flat substrate

First consider the adhesion-induced collapse of a fiber segment on flat substrate. The fiber segment is assumed to be fixed at a distance h evenly to the flat substrate, with length L and radius r, as shown in Figure 2(a). The fiber material is regarded as linearly isotropic elastic with Young's modulus E. At sufficiently small distance h, subjected to small perturbation (*e.g.*, air flow, dust collision, etc.), the fiber segment may collapse and stick to the substrate due to the adhesive force, as illustrated in Figure 2(b). At the critical condition of one-point contact, deflection of the mid-span of the fiber segment is h, as shown in Figure 2(c). Based on elementary Euler–Bernoulli beam theory, the deflection v and corresponding adhesive force P required in inducing the collapse can be expressed as

$$v = 3h\left[\left(\frac{2x}{L}\right)^2 - \frac{2}{3}\left(\frac{2x}{L}\right)^3\right], \tag{1}$$

$$P = \frac{48\pi E r^4 h}{L^3}. \tag{2}$$

In the above, due to the symmetry of the fiber deflection, x can be understood as the distance from an arbitrary point on the fiber segment to the fixed support or equivalently the distance from that to the contact point, as shown in Figure 2(c). Relation (2) is to be used in determining the critical collapse distance h_c once the adhesive force P is esti-

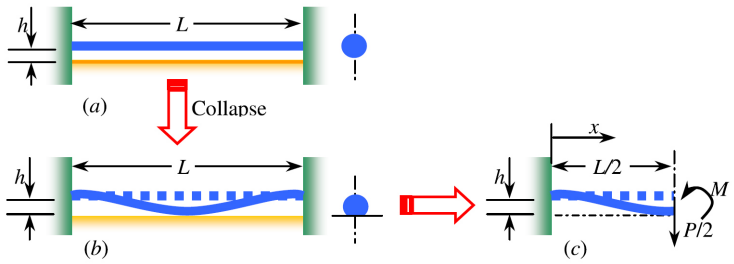

Figure 2. Adhesion between fiber segment and flat substrate.

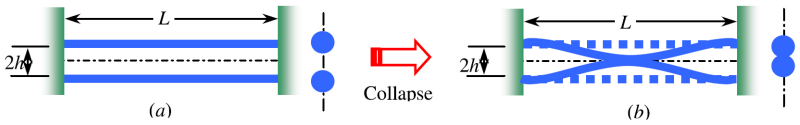

Figure 3. Adhesion between parallel fiber segments.

mated. As we know, the adhesive forces between two fiber segments are actually distributed. However, they can be replaced by their resultant P due to the rapidly decaying characteristic of the adhesive force with increasing gap between two fibers near the contact point. Furthermore, the adhesive force P can be directly calculated using Bradley's approach [35], which is based on the long-range Lennard-Jones force between two unit areas [42], *i.e.*,

$$\sigma(z) = \frac{8\Delta\gamma}{3\varepsilon}\left[\left(\frac{\varepsilon}{z}\right)^3 - \left(\frac{\varepsilon}{z}\right)^9\right]. \tag{3}$$

Here, ε is a phenomenological distance between two atoms/molecules; z is the distance between two unit areas; and $\Delta\gamma$ is the Dupré adhesion energy [43] that is defined as

$$\Delta\gamma = \gamma_1 + \gamma_2 - \gamma_{12}, \tag{4}$$

where γ_1 and γ_2 are, respectively, the surface energies of the nanofiber and the substrate and γ_{12} is the interface energy between the nanofiber and the flat substrate. According to Bradley's approach [35], the deflected nanofiber segment can be regarded as rigid at the critical condition of one-point contact (see Figure 2(c)). Therefore, with the aid of the deflection shape (1), the asymptotic distance between the deflected fiber segment and the flat substrate near the contact point can be expressed as

$$\begin{aligned} z &= 3h\left[\left(\frac{2x}{L}\right)^2 - \frac{2}{3}\left(\frac{2x}{L}\right)^3\right] + \frac{y^2}{2r} + h_0 \\ &\approx 3h\left(\frac{2x}{L}\right)^2 + \frac{y^2}{2r} + h_0, \qquad (\text{for } x/L \ll 1) \end{aligned} \tag{5}$$

where h_0 is the minimum gap at the contact point after collapse, which can be selected as $h_0 = \varepsilon$ according to Bradley's approach [35]. x and y are the coordinates of an arbitrary point on the substrate with x axis along the fiber axis and y axis perpendicular to the fiber axis in the horizontal plane. As a result, the adhesive force P can be determined:

$$\begin{aligned} P &= 4\int_A \sigma(z)\,\mathrm{d}A \\ &= \frac{32\Delta\gamma}{3\varepsilon}\int_0^{+\infty}\int_0^{+\infty}\left[\left(\frac{\varepsilon}{z}\right)^3 - \left(\frac{\varepsilon}{z}\right)^9\right]\mathrm{d}x\,\mathrm{d}y, \\ &= \frac{\pi}{\sqrt{6}}\Delta\gamma L\sqrt{r/h}, \end{aligned} \tag{6}$$

where geometrical symmetry of the contact zone and $h_0 = \varepsilon$ have been implied. Substituting (6) into (2) yields the critical collapse distance h_c:

$$\left(\frac{h_c}{L}\right)^{3/2} = \frac{1}{48\sqrt{6}}\frac{\Delta\gamma}{Er}\left(\frac{L}{r}\right)^{5/2}. \tag{7}$$

The above relation has a size effect due to the material intrinsic length $\Delta\gamma/E$ involved.

2.2. Collapse of parallel nanofiber segments

In this case, a pair of uniform fiber segments is considered. Similar to the above derivation, the asymptotic distance between deflected fiber segments (see Figure 3) near the contact point can be expressed as

$$\begin{aligned} z &= 6h\left[\left(\frac{2x}{L}\right)^2 - \frac{2}{3}\left(\frac{2x}{L}\right)^3\right] + \frac{y^2}{r} + h_0 \\ &\approx 6h\left(\frac{2x}{L}\right)^2 + \frac{y^2}{r} + h_0, \qquad (\text{for } x/L \ll 1) \end{aligned} \tag{8}$$

where the (x, y)-coordinate system is selected following that in Section 2.1. By using the adhesive force (6), it is

$$P = 4\int_A \sigma(z)\,\mathrm{d}A = \frac{\pi}{2\sqrt{6}}\Delta\gamma L\sqrt{r/h}. \tag{9}$$

Substituting (9) into (2) leads to the critical collapse distance h_c:

$$\left(\frac{h_c}{L}\right)^{3/2} = \frac{1}{96\sqrt{6}}\frac{\Delta\gamma}{Er}\left(\frac{L}{r}\right)^{5/2}. \tag{10}$$

For uniform fiber segments (*i.e.*, $\gamma_1 = \gamma_2 = \gamma$ and $\gamma_{12} = 0$), the Dupré adhesion energy is reduced to $\Delta\gamma = 2\gamma$ and relation (10) becomes

$$\left(\frac{h_c}{L}\right)^{3/2} = \frac{1}{48\sqrt{6}}\frac{\gamma}{Er}\left(\frac{L}{r}\right)^{5/2}. \tag{11}$$

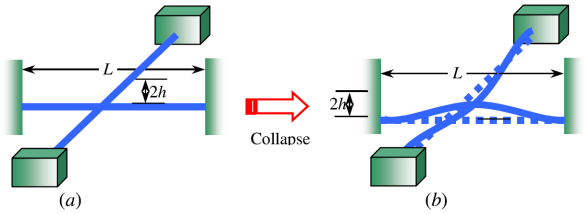

Figure 4. Adhesion between orthogonal fiber segments.

2.3. Collapse of orthogonal nanofiber segments

In this case, two fiber segments are still considered with the same geometries and material properties. Thus, the deflection shape (1) still holds for each fiber segment as illustrated in figure 4. Based on the derivation in Section 2.1, the asymptotic distance between deflected fiber segments near the contact point is

$$\begin{aligned} z &= 3h\left[\left(\frac{2x}{L}\right)^2 - \frac{2}{3}\left(\frac{2x}{L}\right)^3\right] + 3h\left[\left(\frac{2y}{L}\right)^2 - \frac{2}{3}\left(\frac{2y}{L}\right)^3\right] \\ &\quad + \frac{x^2}{2r} + \frac{y^2}{2r} + h_0 \\ &\approx \left(\frac{12h}{L^2} + \frac{1}{2r}\right)(x^2 + y^2) + h_0 \\ &\quad (\text{for } x/L \ll 1 \text{ and } y/L \ll 1). \end{aligned} \tag{12}$$

Substituting (12) into (6) yields the adhesive force:

$$P = 4\int_A \sigma(z)\,\mathrm{d}A = \frac{2\pi\Delta\gamma r}{1 + 24hr/L^2}. \tag{13}$$

In the limiting case of two long, straight, rigid cylinders (*i.e.*, $L \gg r$ or $L \gg h$), relation (13) covers those estimated using the Derjaguin approximation [44]. Consequently, plugging (13) into (2) leads to the quadratic characteristic equation of the system such that

$$\left(\frac{h}{L}\right)^2 + \frac{L}{24r}\left(\frac{h}{L}\right) - \frac{\Delta\gamma L^3}{24^2 E r^4} = 0. \tag{14}$$

The positive root of (14) gives the critical collapse distance h_c:

$$\frac{h_c}{L} = \frac{1}{48}\left[\sqrt{\left(\frac{L}{r}\right)^2 + \frac{4\Delta\gamma L^3}{Er^4}} - \frac{L}{r}\right]. \tag{15}$$

With the Dupré adhesion energy $\Delta\gamma = 2\gamma$ in this case, relation (15) can be recast into

$$\frac{h_c}{L} = \frac{1}{48}\left[\sqrt{\left(\frac{L}{r}\right)^2 + \frac{8\gamma L^3}{Er^4}} - \frac{L}{r}\right]. \tag{16}$$

Furthermore, for relatively large fiber radius, there exists a limiting critical collapse distance dependent only of the fiber aspect ratio L/r and the material intrinsic length (usually $\gamma/E < 1$ nm) such that

$$h_c = \frac{1}{12}\left(\frac{L}{r}\right)^3 \frac{\gamma}{E}. \tag{17}$$

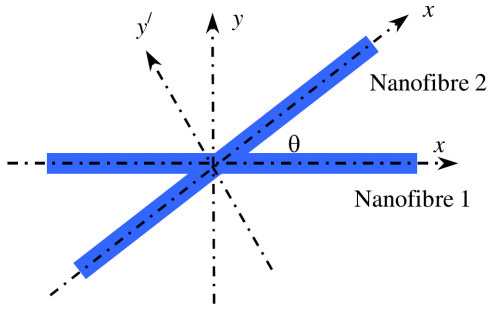

Figure 5. Geometries of fibers at arbitrary angle.

2.4. Collapse of fiber segments in arbitrary angle

Now let us consider two uniform fiber segments located in two parallel horizontal planes with distance h. The spatial angle between the fiber axes is denoted as θ. Simple relationships exist between two coordinate systems attached to the fiber axes as adopted in Figure 5:

$$\begin{aligned} x' &= x\cos\theta + y\sin\theta, \\ y' &= -x\sin\theta + y\cos\theta. \end{aligned} \tag{18}$$

Obviously, in the first-order approach, the deflection shape (1) still holds for each nanofiber segment after collapse. By using the derivation in Section 2.1, the asymptotic distance between deflected fiber segments near the contact point is

$$\begin{aligned} z &= 3h\left[\left(\frac{2x}{L}\right)^2 - \frac{2}{3}\left(\frac{2x}{L}\right)^3\right] + \frac{y^2}{2r} + 3h \\ &\quad \times \left[\left(\frac{2x'}{L}\right)^2 - \frac{2}{3}\left(\frac{2x'}{L}\right)^3\right] + \frac{y'^2}{2r} + h_0 \\ &\approx \frac{12h}{L^2}x^2 + \frac{y^2}{2r} + \frac{12h}{L^2}x'^2 + \frac{y'^2}{2r} + h_0 \\ &\quad (\text{for } x/L \ll 1 \text{ and } x'/L \ll 1) \end{aligned} \tag{19}$$

Substituting (18) into (19) yields the asymptotic distance in the (x, y) system such that

$$\begin{aligned} z &\approx \frac{12h}{L^2}\left[(1+\cos^2\theta)x^2 + \sin 2\theta xy + \sin^2\theta y^2\right] \\ &\quad + \frac{1}{2r}\left[\sin^2\theta x^2 - \sin 2\theta xy + (1+\cos^2\theta)y^2\right] + h_0 \\ &\quad (\text{for } x/L \ll 1 \text{ and } x'/L \ll 1) \end{aligned} \tag{20}$$

In the above, if letting $\theta = 0°$ and $\theta = 90°$, the asymptotic distance (20) recovers the ones given by (8) and (12), respectively. Furthermore, by using (20) to replace the distance z in (6), one can obtain the adhesive force:

$$\begin{aligned} P &= \int_\Gamma \sigma(z)\,\mathrm{d}A = \frac{8\Delta\gamma}{3\varepsilon}\int_{-\infty}^{+\infty}\int_{-\infty}^{+\infty}\left[\left(\frac{\varepsilon}{z}\right)^3 - \left(\frac{\varepsilon}{z}\right)^9\right]\mathrm{d}x\,\mathrm{d}y, \\ &= \pi\Delta\gamma L/\sqrt{D}, \end{aligned} \tag{21}$$

where D is the determinant of a positive-defined matrix relating the fiber aspect ratio L/r, fiber distance h_c and angle between fibers θ, *i.e.*,

$$D = \begin{vmatrix} (1+\cos^2\theta)\frac{12h}{L} + \sin^2\theta\frac{L}{2r} & \sin\theta\cos\theta\left(\frac{12h}{L} + \frac{L}{2r}\right) \\ \sin\theta\cos\theta\left(\frac{12h}{L} + \frac{L}{2r}\right) & \sin^2\theta\frac{12h}{L} + (1+\cos^2\theta)\frac{L}{2r} \end{vmatrix}. \tag{22}$$

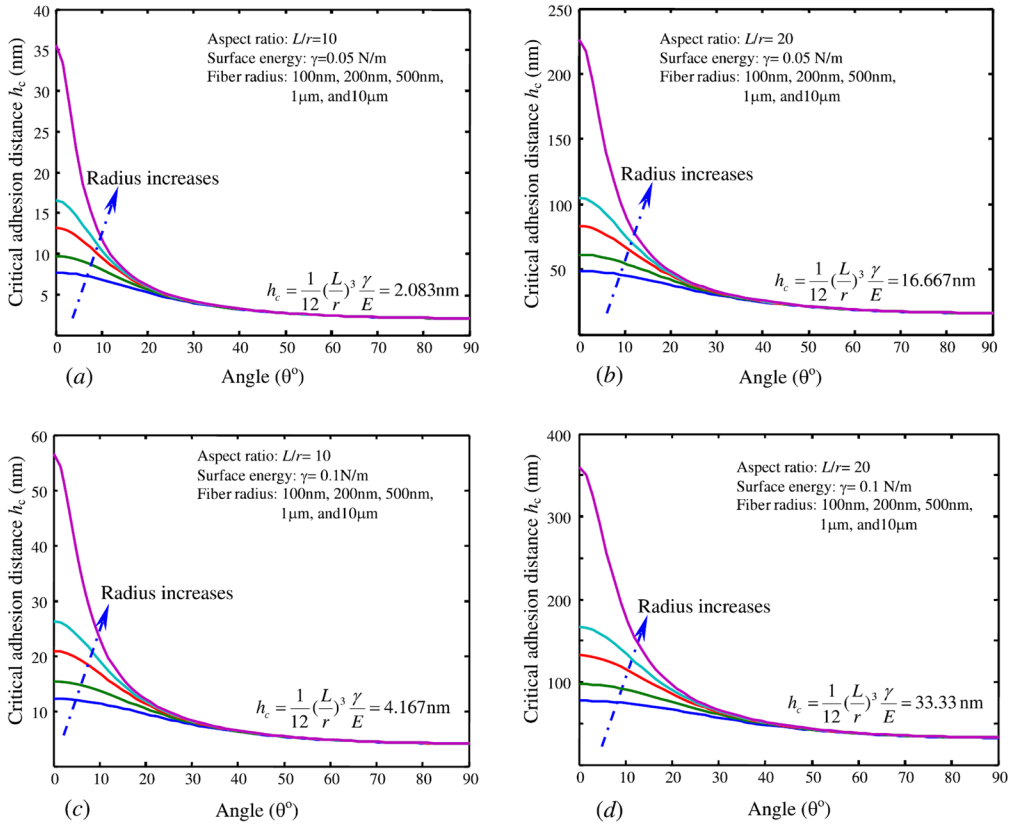

Figure 6. Variation of the critical collapse distance h_c between fiber segments versus angle θ at varying fiber radius r and aspect ratio L/r : (**a**) $L/r = 10$, $\gamma = 0.05$ N m^{-1}; (**b**) $L/r = 20$, $\gamma = 0.05$ N m^{-1}; (**c**) $L/r = 10$, $\gamma = 0.1$ N m^{-1}; and (**d**) $L/r = 20$, $\gamma = 0.1$ N m^{-1}.

Plugging (21) into (2) leads to the characteristic equation of the system such that

$$\frac{h_c}{L} = \frac{1}{48\sqrt{D}} \frac{\Delta\gamma}{Er} \left(\frac{L}{r}\right)^3. \tag{23}$$

Again, with the Dupré adhesion energy $\Delta\gamma = 2\gamma$ in this case, relation (23) can be rewritten as

$$\frac{h_c}{L} = \frac{1}{24\sqrt{D}} \frac{\gamma}{Er} \left(\frac{L}{r}\right)^3. \tag{24}$$

In the above, except for the special cases of $\theta = 0°$ and 90° as discussed in Sections 2.2 and 2.3, for an arbitrary angle θ, it is unable to extract the critical collapse distance h_c in explicit form from (24). In this case, the numerical method for searching roots of polynomials has to be evoked.

3. Numerical results and discussions

With critical collapse criterion (24) involving the material intrinsic length γ/E or $\Delta\gamma/E$, we can draw the conclusion that the size effect of fiber radius on nanofiber collapse does exist. Hereafter, we evaluate the variation of the critical collapse distance hc versus the fiber angle θ at varying surface energy γ, fiber aspect ratio L/r and fiber radius r. For convenience, relation (24) is recast into

$$\frac{h_c}{r} = \frac{1}{24\sqrt{D}} \frac{\gamma}{Er} \left(\frac{L}{r}\right)^4. \tag{25}$$

During the numerical process, fiber surface energies are selected as $\gamma = 0.05$ N m^{-1} and $\gamma = 0.1$ N m^{-1}, respectively, and Young's modulus is chosen as $E = 2$ GPa. These values are close to those of typical polymer fibers. Therefore, once parameters L, r and θ are given, equation (25) can be solved numerically for h_c. The h_c values for fiber segments of radii 100 nm, 200 nm, 500 nm, 1 μm, and 10 μm, respectively, are plotted in Figure 6, from which it can be found that the size effect of fiber radius exists. For a given fiber pair, the critical collapse distance h_c decreases rapidly with increasing angle θ, and simultaneously it also decreases with the increase of fiber surface energy. At fixed fiber aspect ratio L/r, at small angle θ, h_c increases with increasing fiber radius; however, at relatively large angle θ, h_c tends to a constant as given in (17), *e.g.* $(1/12)\ (L/r)^3\ \gamma/E$. This constant depends only upon the aspect ratio L/r and the material intrinsic length $\gamma/E = 0.025$ nm for $\gamma = 0.05$ N m^{-1}, and $\gamma/E = 0.05$ nm for $\gamma = 0.1$ N m^{-1}. This parameter is expected to be very useful for collapse analysis and design of nanofiber networks and nanofiber devices. Furthermore, at fixed fiber radius, h_c grows significantly with increasing aspect ratio L/r. This is because the bending stiffness of a fiber segment decreases rapidly with the increase of fiber segment length following a reciprocal cubic law.

In reality, nanofiber segments within a fiber network usually have very high aspect ratio. Due to the small diameter of nanofibers, the above analysis implies that nanofiber networks are generally more unstable than those made of thick fibers. Numerical simulation also indicates that parallel fibers have the maximum h_c value due to their greatest

adhesive force, while orthogonal fibers have the minimum h_c value. This is a reasonable explanation of the nanofiber collapse phenomena observed in experiments.

Nevertheless, it should be mentioned that surface adhesion in a real fiber network is much more complex. In particular, near the fiber contacts where two or more fibers intersect, the adhesion calculation would be more complicated. Fixed boundary conditions adopted above are also a strict assumption. Consequently, all the above calculations of adhesive force are based on a modified Bradley's approach; therefore the adhesion energy of post-collapse (with greater contact areas) is much greater than the initial adhesion energy in inducing the initial nanofiber collapse (adhesion) of nanofibers as considered in this work.

4. Conclusions

In this paper, adhesion-induced micro/nanofiber collapse has been studied. The critical collapse distance between neighboring fiber segments has been derived for typically four fiber collapse modes. Relation (24) is the general criterion for adhesion-induced collapse of fibers. Based on this relation, effects of fiber elasticity, surface adhesion and fiber geometries on the critical collapse distance have been explored. Due to the involvement of the material's intrinsic length $\Delta\gamma/E$ or γ/E in (23) and (24), the fiber collapse condition has a size effect. The calculation of the adhesive force in the present study is based on Bradley's approach, which does not consider the deformation induced by adhesion. However, this approach did not affect the present results for only considering the critical condition of initial fiber collapse.

Furthermore, although the present study is based on two uniform micro/nanofiber segments, the method developed above can be naturally extended in examining the collapse mechanisms and criteria of micro/nanofiber networks made of dissimilar fibers (*e.g.*, with dissimilar material properties, geometries, etc) and other microstructures such as MEMS/NEMS and slender rubber stamps used in soft lithography.

Acknowledgments

Partial support of this study by the U.S. NSF, AFOSR, and ARO/ARL is gratefully acknowledged. The authors would like to thank the anonymous reviewers from *Nanotechnology* for their enlightening comments and helpful suggestions to improve the paper.

References

[1] Reneker D H and Chun I 1996 *Nanotechnology* **7** 216
[2] Dzenis Y 2004 *Science* **304** 1917
[3] Li D and Xia Y N 2004 *Adv. Mater.* **16** 1151
[4] Huang C B, Chen S L, Lai C L, Reneker D H, Qiu H, Ye Y, and Hou H Q 2006 *Nanotechnology* **17** 1558
[5] Kim J S and Reneker D H 1999 *Polym. Compos.* **20** 124
[6] Dzenis Y A and Reneker D H 2001 US Patent Specification 626533
[7] Dzenis Y A and Wen Y K 2002 *Mater. Res. Soc. Symp. Proc.* **702** 173
[8] Wu X F 2003 Fracture of advanced polymer composites with nanofiber reinforced interfaces PhD Thesis University of Nebraska–Lincoln, Lincoln, NE, U.S.A.
[9] Huang Z M, Zhang Y Z, Kotaki M, and Ramakrishna S 2003 *Compos. Sci. Technol.* **63** 2223
[10] Zhang Y Z, Lim C T, Ramakrishna S, and Huang Z M 2005 *J. Mater. Sci. Mater. Med.* **16** 933
[11] Chew S Y, Wen Y, Dzenis Y, and Leong K W 2006 *Curr. Pharm. Des.* **12** 4751
[12] van Wyk C M 1946 *J. Textile Inst.* **37** T285
[13] Cox H L 1952 *Brit. J. Appl. Phys.* **3** 72
[14] Pan N and Carnaby G A 1989 *Textile Res. J.* **59** 285
[15] Carnaby G A and Pan N 1989 *Textile Res. J.* **59** 275
[16] Komori T and Itoh M 1991 *Textile Res. J.* **61** 420
[17] Komori T and Itoh M 1991 *Textile Res. J.* 61 588
[18] Komori T, Itoh M, and Takaku A 1992 *Textile Res. J.* **62** 567
[19] Lee D H and Carnaby G A 1992 *Textile Res. J.* **62** 185
[20] Niskanen K J and Alava M J 1994 *Phys. Rev. Lett.* **73** 3475
[21] Astrom J, Saarinen S, Niskanen K, and Kurkijarvi J 1994 *J. Appl. Phys.* **75** 2383
[22] Pan N, Chen J, Seo M, and Backer S 1997 *Textile Res. J.* **67** 907
[23] Wang C, Cheng X, Sastry A M, and Choi S B 1999 *ASME J. Eng. Mater. Technol.* **121** 503
[24] Narter M A, Batra S K, and Buchanan D R 1999 *Proc. R. Soc. A* **455** 3543
[25] Astrom J A, Makinen J P, Alava M J, and Timonen J 2000 *Phys. Rev. E* **61** 5550
[26] Astrom J A, Makinen J P, Hirvonem H, and Timonen J 2000 *J. Appl. Phys.* **88** 5056
[27] Wang C W, Berhan L, and Sastry A M 2000 *ASME J. Eng. Mater. Technol.* **122** 450
[28] Wang C W and Sastry A M 2000 *ASME J. Eng. Mater. Technol.* **122** 460
[29] Sastry A M, Wang C W, and Berhan L 2001 *Key Eng. Mater.* **200** 229
[30] Berhan L, Yi Y B, and Sastry A M 2004 *J. Appl. Phys.* **95** 5027
[31] Berhan L, Yi Y B, Sastry A M, Munoz E, Selvidge M, and Baughman R 2004 *J. Appl. Phys.* **95** 4335
[32] Wu X F and Dzenis Y A 2005 *J. Appl. Phys.* **98** 093501
[33] Chatterjee A P 2006 *J. Appl. Phys.* **100** 054302
[34] Wu X F and Dzenis Y A 2006 *J. Appl. Phys.* **100** 124318
[35] Bradley R S 1932 *Phil. Mag.* **13** 853
[36] Johnson K L, Kendall K, and Roberts A D 1971 *Proc. R. Soc. A* **324** 301
[37] Derjaguin B V, Muller V M, and Toporov Y P 1975 *J. Colloid Interface Sci.* **53** 314
[38] Tabor D 1977 *J. Colloid Interface Sci.* **58** 2
[39] Greenwood J A 1997 *Proc. R. Soc. A* **453** 1277
[40] Zhao Y P, Wang L S, and Yu T X 2003 *J. Adhes. Sci. Technol.* **17** 519
[41] Shi X H and Zhao Y P 2004 *J. Adhes. Sci. Technol.* **18** 55
[42] Muller V M, Yushchenko V S, and Derjaguin B V 1980 *J. Colloid Interface Sci.* **77** 91
[43] Maugis D 1992 *J. Colloid Interface Sci.* **150** 243
[44] Israelachvili J 1992 *Intermolecular and Surface Forces* 2nd edition (New York: Academic)